Reproducible mesoscopic superpositions of Bose-Einstein condensates and mean-field chaos

Bettina Gertjerenken,* Stephan Arlinghaus, Niklas Teichmann, and Christoph Weiss
Institut für Physik, Carl von Ossietzky Universität, D-26111 Oldenburg, Germany
(Received 11 January 2010; published 30 August 2010)

In a parameter regime for which the mean-field (Gross-Pitaevskii) dynamics becomes chaotic, mesoscopic quantum superpositions in phase space can occur in a double-well potential, which is shaken periodically. For experimentally realistic initial states, such as the ground state of some 100 atoms, the emergence of mesoscopic quantum superpositions in phase space is investigated numerically. It is shown to be reproducible, even if the initial conditions change slightly. Although the final state is not a perfect superposition of two distinct phase states, the superposition is reached an order of magnitude faster than in the case of the collapse-and-revival phenomenon. Furthermore, a generator of entanglement is identified.

DOI: 10.1103/PhysRevA.82.023620 PACS number(s): 03.75.Gg, 05.45.Mt, 03.75.Lm

I. INTRODUCTION

Periodically shaking potentials used to trap ultracold atoms currently is established as an experimental method [1–3]: Tunneling has been suppressed by choosing the correct amplitude of driving both for a Bose-Einstein condensate (BEC) in an optical lattice [1,4,5] and for a single atom in a double-well potential [3,6]. By fine-tuning the driving frequency, tunneling in tilted systems can also be enhanced in an analog of photon-assisted tunneling. After the driving frequency has helped to bridge potential differences, tunneling can again be controlled by tuning the driving amplitude [2,4,7]. BECs in periodically driven systems have been investigated with regard to tunneling [8,9], dynamic localization [5], and stabilities of exact Floquet states [10].

Suggestions about how mesoscopic superpositions, such as the $N00N$ state [11],

$$|\Psi\rangle \equiv \frac{1}{\sqrt{2}}(|N,0\rangle + |0,N\rangle), \tag{1}$$

could be obtained with BECs can be found in Refs. [12–26]; for a BEC in a double well, this corresponds to a quantum superposition of all N particles, which are either in one well or in the other. Here, $|n,N-n\rangle$ denotes the Fock state with n particles in the left well and $N-n$ particles in the right well. Like the spin-squeezed states investigated in Refs. [27–29], such states are relevant to improve interferometric measurements [30].

A promising approach for obtaining mesoscopic superpositions is the collapse-and-revival phenomenon in phase space if the tunneling between both wells of a double-well potential is suppressed (or, for a single-species condensate in a harmonic trapping potential, the transition between two hyperfine states). A $N00N$ state then appears on the time scale [31],

$$t_0 = \frac{\pi}{4\kappa}, \tag{2}$$

where $2\hbar\kappa$ is the interaction energy of a pair of atoms. Chaos-induced entanglement generation in a periodically shaken double well should, in principle, offer the possibility for obtaining mesoscopic superpositions on short time scales [32]. While the state will not be a perfect superposition, the time scale on which it is reached will be an order of magnitude smaller. In this paper, the question is whether these superpositions can be achieved both for experimentally realistic conditions and for parameters such that the superposition is reproducible: In an experiment, the particle number will vary from shot to shot, and the tilt in a double well or the amplitude of shaking is likely to be slightly different.

The paper is organized as follows. Section II introduces the model used to describe a BEC in a periodically shaken double well. Section III describes experimental signatures of the entangled states. In Sec. IV, a generator of mesoscopic superpositions is discussed, while Sec. V demonstrates that the generation of mesoscopic quantum superpositions is robust against slight changes in the initial conditions.

II. A BEC IN A PERIODICALLY SHAKEN DOUBLE WELL

BECs in double-well potentials are interesting both experimentally and theoretically [12,28,33–37]. In order to describe a BEC in a double well, we use a model originally developed in nuclear physics [38]: a many-particle Hamiltonian in two-mode approximation [39],

$$\hat{H} = -\frac{\hbar\Omega}{2}(\hat{c}_1^\dagger\hat{c}_2 + \hat{c}_2^\dagger\hat{c}_1) + \hbar\kappa(\hat{c}_1^\dagger\hat{c}_1^\dagger\hat{c}_1\hat{c}_1 + \hat{c}_2^\dagger\hat{c}_2^\dagger\hat{c}_2\hat{c}_2) + \hbar[\mu_0 + \mu_1\sin(\omega t)](\hat{c}_2^\dagger\hat{c}_2 - \hat{c}_1^\dagger\hat{c}_1), \tag{3}$$

where the operator $\hat{c}_j^{(\dagger)}$ annihilates (creates) a boson in well j; $\hbar\Omega$ is the tunneling splitting, $2\hbar\mu_0$ is the tilt between well 1 and well 2, and $\hbar\mu_1$ is the driving amplitude. The interaction energy of a pair of particles in the same well is denoted by $2\hbar\kappa$.

The Gross-Pitaevskii dynamics can be mapped to that of a nonrigid pendulum [34]. By including the term, which describes the periodic shaking, the classical Hamiltonian is given by

$$H_{\mathrm{mf}} = \frac{N\kappa}{\Omega}z^2 - \sqrt{1-z^2}\cos(\phi) - 2z\left[\frac{\mu_0}{\Omega} + \frac{\mu_1}{\Omega}\sin\left(\frac{\omega}{\Omega}\tau\right)\right], \quad \tau = t\Omega, \tag{4}$$

where z is the population imbalance, where $z=1$ ($z=-1$) refers to the situation with all particles in well 1 (well 2).

*gertjerenken@theorie.physik.uni-oldenburg.de

On the N-particle quantum level, if all atoms occupy the single-particle state characterized by $z = \cos(\theta)$ and ϕ, this leads to the wave function

$$|\theta,\phi\rangle = \sum_{n=0}^{N} \binom{N}{n}^{1/2} \cos^n(\theta/2)\sin^{N-n}(\theta/2) \times e^{i(N-n)\phi}|n,N-n\rangle. \quad (5)$$

These bimodal phase states [31] are sometimes referred to as atomic coherent states. Note that, for finite N, these are not orthogonal:

$$|\langle\theta,\phi\,|\theta',\phi'\rangle|^2 > 0, \qquad N < \infty. \quad (6)$$

As the Gross-Pitaevskii dynamics corresponds to that of a nonrigid pendulum, the dynamics is known to display a coexistence between chaotic and regular regions [40]. Here, the relation to entanglement [32] is discussed (cf. [41,42] for the δ-kicked top).

III. SIGNATURES OF MESOSCOPIC QUANTUM SUPERPOSITIONS

The signatures of entangled states described in this section can only serve as signatures of entangled states [43] if they are followed by a revival. However, as these revivals are only partial, this will not be a proof of entanglement but, nevertheless, a strong indication. Furthermore, on the level of computer simulations, one does not have the necessity to distinguish between quantum superpositions and statistical mixtures. Further information, which concerns the states of interest, the superposition of atomic coherent states (5), can be found in Ref. [32].

Here, one signature of entanglement is the quantum Fisher information [44,45], for the relative phase between the condensates in the two potential wells (in the following referred to as the QFI). By defining for pure states,

$$F_{\mathrm{QFI}} \equiv (\Delta n_{12})^2, \quad (7)$$

where $(\Delta n_{12})^2$ is the experimentally measurable [28] variance of the particle-number difference between both wells, one has an entanglement flag. For pure states,

$$F_{\mathrm{ent}} > 1, \qquad F_{\mathrm{ent}} \equiv \frac{F_{\mathrm{QFI}}}{N} \quad (8)$$

is a sufficient condition for particle entanglement and identifies those entangled states that are useful for overcoming classical phase sensitivity in interferometric measurements [44]. By defining entangled states as states, which cannot be written as product states [31], this statement is supported by the fact that, for a single atomic coherent state (5), one has $F_{\mathrm{ent}} \leqslant 1$. This is expected, since, in this case, all atoms occupy the same single-particle state. For mixtures, the QFI becomes more complicated (Ref. [44] and references therein) and might not be easy to measure. To take the definition of Eq. (7) for an experiment, leaves the difficulty of distinguishing superpositions from mixtures.

Another experimental signature [46] will be provided by interference patterns after switching off the potential and letting the wave function expand for some time. A single atomic coherent state $|\theta,\phi\rangle$ leads to an interference pattern used to experimentally detect the phase between the condensates [33],

$$I(X) = [1 + \sin(\theta)\cos(X-\phi)], \quad (9)$$

which still has to be multiplied by a Gaussian envelope; X essentially is the spatial variable in the direction, which connects the two wells of the double well, and I is the intensity at X. To characterize the quality of interference fringes, the visibility or contrast,

$$C \equiv \frac{I_{\max} - I_{\min}}{I_{\max} + I_{\min}}, \quad (10)$$

is introduced, where $I_{\max}$ is the highest and $I_{\min}$ is the lowest value of I. Given the fact that, even a single atomic coherent state can produce an impressive interference pattern, interference cannot be used in a straightforward manner as an entanglement flag as in Refs. [23,36]. Thus, let us consider the *disappearance* of interference patterns,

$$C \ll 1. \quad (11)$$

This might simply mean $\sin(\theta) \simeq 0$ [cf. Eq. (9)] or even heating. However, when combined with a high QFI, it will be the signature for the superposition of two (or more) distinct atomic coherent states with $\sin(\theta_1) \simeq \sin(\theta_2)$ and $\cos(X-\phi_1) + \cos(X-\phi_2) = 0$. This is a strong indication for mesoscopic superpositions similar to the case of the superfluid-to-Mott-insulator transition [47] where the disappearance and reappearance of the contrast clearly indicates (but does not prove) the Mott-insulator transition.

In order to numerically calculate the contrast, one needs [48]

$$\langle\psi|\hat{\Psi}^\dagger(x)\hat{\Psi}(x)|\psi\rangle, \quad (12)$$

with

$$\hat{\Psi}(x) = \Phi_1(x)\hat{c}_1 + \Phi_2(x)\hat{c}_2, \quad (13)$$

where Φ_i is the expanded mode, which was originally localized in well i with $i = 1,2$ before switching off the potential.

IV. EMERGENCE OF QUANTUM SUPERPOSITIONS

The claim of Ref. [32] is not that mean-field chaos is the origin of entanglement generation but rather that it speeds up the emergence of mesoscopic superpositions. Thus, rather than looking for entanglement generators, which are only present in mean-field chaos, at least some of the aspects should be understandable in a parameter regime for which the mean-field dynamics is regular; and, thus, the corresponding Poincaré surface of section [cf. Fig. 1(a)] is easy to understand: Essentially, there is one elliptic fixed point at $z \approx 0.17$, $\phi \approx -0.48\pi$ and one hyperbolic fixed point near $z \approx 0.21$ and $\phi \approx 0.54\pi$. In addition, there are further fixed points near the top and bottom of the plot, which can be discarded at this point. Within the mean-field dynamics, a solution that starts right on a hyperbolic fixed point $(\theta_{\mathrm{hyper}},\phi_{\mathrm{hyper}})$ will not move at all. This, however, is different on the N-particle quantum level: The N-particle state $|\theta_{\mathrm{hyper}},\phi_{\mathrm{hyper}}\rangle$ will—for any $N < \infty$—have contributions from neighboring atomic coherent states [cf. Eq. (6)]. Those states, even on the mean-field level, do move.

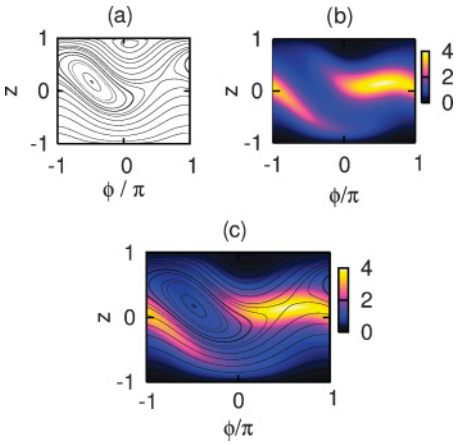

FIG. 1. (Color online) Comparison of the Poincaré surface of section (a) and the QFI map (b) for parameters $2\mu_0/\Omega = 3.0$, $N\kappa/\Omega = 0.5$, $\omega/\Omega = 3.0$, and $2\mu_1/\omega = 0.1$. Plot (b) shows the time-averaged QFI for a system with $N = 100$ particles and averaging time $10/\Omega$. The QFI is enhanced close to the hyperbolic fixed point in the Poincaré surface of section ($z \approx 0.21$, $\phi \approx 0.54\pi$), which acts as a generator of mesoscopic entanglement (c).

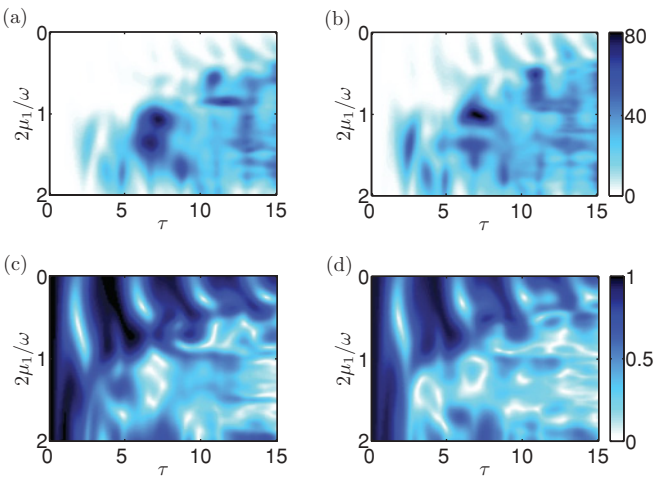

FIG. 2. (Color online) Entanglement flag F_{ent} as a function of time $\tau = \Omega t$ and scaled driving amplitude $2\mu_1/\omega$ for (a) the ground and (b) the first excited state. (c) and (d): Contrast for the ground and the first excited state. $N = 110$, $N\kappa/\Omega = 1.045$, $\mu_0/\Omega = 0.75$, and $\omega/\Omega = 3.0$.

Figure 1(b) shows the time-averaged QFI of all particles, which initially occupy an atomic coherent state. For starting values in the vicinity of the hyperbolic fixed point mentioned previously, mesoscopic superpositions occur. If this is indeed what is happening, the remaining question is why the other hyperbolic fixed points do not display such behavior: In contrast to the first one, they do not lie near the separatrix for which the dynamics happens on much shorter time scales.

Related to the observed acceleration of entanglement generation is the identification of enhanced atomic tunneling between the two wells in high-chaoticity regions [49].

V. ROBUSTNESS OF ENTANGLEMENT GENERATION

In this section, parameters are presented where an entangled state occurs on short time scales, indicated by both signatures QFI and contrast. The robustness of this state under realistic experimental conditions is discussed. In the following, the initial state is prepared without driving, hence, corresponds to the thermal occupation of the eigenstates with energies E_i of Hamiltonian (3) exclusive of the last term. In a typical experimental situation, only some energy eigenstates are significantly occupied [28], which could considerably be reduced by working at lower temperatures in the subnano-Kelvin range [50]. The initial state can be prepared in a well-controlled manner, and the experimental parameters are well controlled [28] except for small experimental uncertainties. The occurring fluctuations of the initial particle number are discussed in this section, while particle losses are not analyzed; their effect on phase revivals has been investigated in Ref. [51].

Figure 2 shows the time development of QFI and the contrast for initial ground and first excited state dependent on the scaled driving amplitude $2\mu_1/\omega$. Obviously, both initial states show similar behavior. Parameters, where both QFI and contrast strongly indicate entanglement, are shown in Fig. 3. The QFI takes on a value of 70.5, and the contrast decreases to 1% already at $\tau = 7.1$. Additionally, the contrast reappears a short time later; hence, heating can be excluded in an experiment.

To determine QFI or contrast in an experiment, it has to be repeated several times with the same initial conditions. However, in the laboratory, parameters such as driving frequency ω and tilt $2\hbar\mu_0$ will change slightly from shot to shot. Figure 4 shows the influence of slight deviations on the two entanglement indicators. Another parameter, where deviations will occur, is the initial particle number N. The dependence of the signatures is represented in Fig. 5. For Poissonian distributed initial particle numbers, the signatures are likely to still be visible in the experiment.

So far, we have optimized with respect to interference patterns and fluctuations of the initial particle number N. Other experimentally interesting quantum states are characterized by a bimodal phase distribution with a small standard deviation. By using the completeness relation [52],

$$\mathbf{1} = \frac{N+1}{4\pi} \int d\theta \sin(\theta) \int d\phi |\theta,\phi\rangle\langle\theta,\phi|, \qquad (14)$$

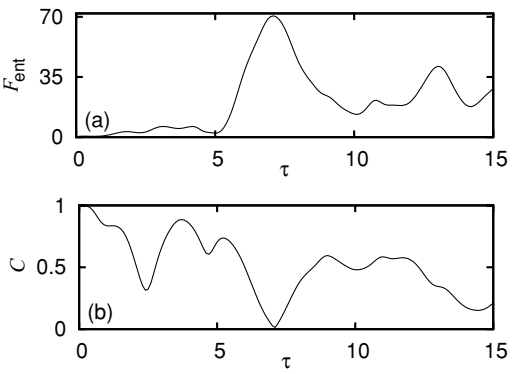

FIG. 3. Entanglement flag (a) F_{ent} and (b) contrast for $2\mu_1/\omega = 1.0$. Other parameters as in Fig. 2.

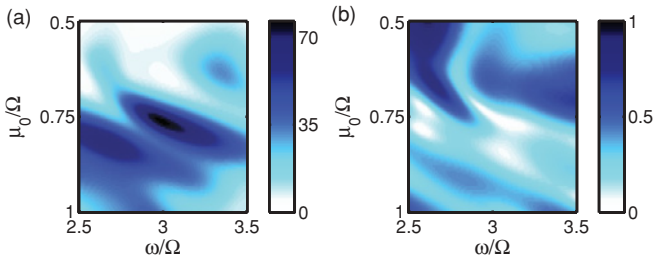

FIG. 4. (Color online) (a) Entanglement flag and (b) contrast at $\tau = 7.1$ versus μ_0/Ω and ω/Ω. $N = 110$, $N\kappa/\Omega = 1.045$, $2\mu_1/\omega = 1.0$.

the phase distribution p_ϕ of a state can be calculated. The initial particle number is again assumed to obey a Poissonian distribution with mean value $N = 110$, which, for numerical purposes, has been truncated and has been renormalized with N, which ranges from $N = 100$ to $N = 120$. Then, a mean-phase distribution and its standard deviation can be calculated for each point of time, which has been optimized in order to find a phase distribution that indicates strong entanglement and has a small standard deviation. In such an optimization procedure, an entangled state has been found at $\tau = 6.5$, where the phase distribution shows two distinct maxima separated by $\Delta\phi \approx \pi$ [cf. Fig. 6(b)]. For maximum reappearance, one important peak is observed at $\tau = 8.9$ (c). For comparison, an exemplary mixed state, which leads to the phase distribution of (b) has been constructed: The wave function at $\tau = 6.5$ has been split into two parts, each consisting of the contributions to p_ϕ in an interval of $\Delta\phi = \pi$ around one of the peaks. In the statistical mixture, these two renormalized parts are weighted according to their contribution to the total wave function. After the corresponding time difference $\Delta\tau = 2.4$, this mixed state would have a phase distribution according to (d), which is distinct from (c). Hence, it is possible to distinguish pure entangled states from mixed states. Additionally, preliminary results indicate that, under slight parameter variations of about 1% for driving frequency, driving strength, and initial tilt, respectively, and about 10% for the scaled interaction strength $N\kappa/\Omega$, the phase distribution at $\tau = 6.5$ and the partial revival at $\tau = 8.9$, nonetheless, stay robust.

In addition to slight changes in the experimental conditions, another effect that should be discussed is the influence of temperature. So far, calculations have been performed for $T = 0$. To account for temperature, the eigenstates of the undriven system, which correspond to energies E_i, are supposed to

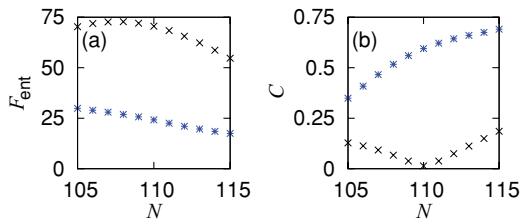

FIG. 5. (Color online) (a) F_{ent} and (b) contrast for $\tau = 7.1$ (black crosses) and $\tau = 9.0$ (blue stars) for different particle numbers such that $\kappa/\Omega = \text{const}$. $N\kappa/\Omega(N = 110) = 1.045$, $\mu_0/\Omega = 0.75$, $\omega/\Omega = 3.0$, and $2\mu_1 = 1.0$.

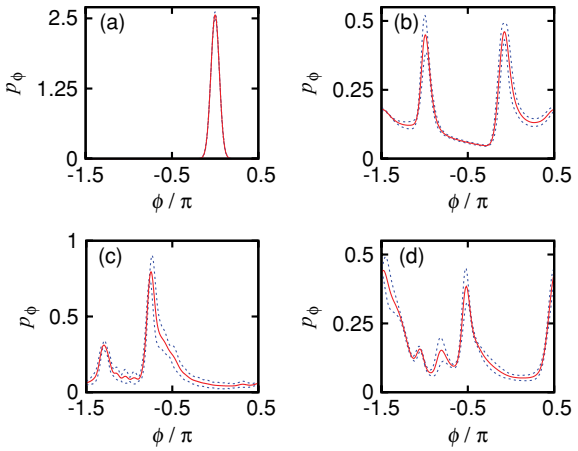

FIG. 6. (Color online) Averaged phase distribution p_ϕ (red solid line) with standard deviation (blue dashed lines). The initial particle number is modeled by a truncated renormalized Poisson distribution of the initial particle number, which ranges from $N = 100$ to $N = 120$, with mean value $N = 110$. (a) Initial state, (b) entangled state at $\tau = 6.5$, (c) time-developed state at $\tau = 8.9$, and (d) assumed exemplary two-component statistical mixture at $\tau = 8.9$. The interaction strength κ/Ω is kept constant such that $N\kappa/\Omega(N = 110) = 1.0$. $\mu_0/\Omega = 1.3$, $\omega/\Omega = 3.3$, and $2\mu_1/\omega = 0.7$.

be populated with probability p_i according to a Boltzmann distribution:

$$p_i = \frac{e^{-(E_i - E_0)/k_B T}}{\mathcal{Z}}, \quad \mathcal{Z} = \sum_{i=0}^{M} e^{-(E_i - E_0)/k_B T}. \tag{15}$$

Hence, the statistically averaged contrast is given by

$$\langle C \rangle_{\text{st}} = \sum_{i=0}^{M} p_i C_i, \tag{16}$$

where C_i is the contrast for the pure state i and M is the number of states included in the average. With an analog definition of $\langle\cdot\rangle_{\text{st}}$, the statistically averaged QFI becomes

$$\langle F_{\text{ent}} \rangle_{\text{st}} = \frac{\langle (\Delta n_{12})^2 \rangle_{\text{st}}}{N} = \frac{1}{N}\left(\langle n_{12}^2 \rangle_{\text{st}} - \langle n_{12} \rangle_{\text{st}}^2 \right). \tag{17}$$

Also, for comparison, the QFI for mixed states (Ref. [44] and references therein),

$$F_{\text{ent,mixed}} = \frac{1}{2N} \sum_{j,k} \frac{(p_j - p_k)^2}{p_j + p_k} |\langle j | n_{12} | k \rangle|^2, \tag{18}$$

again, relative to the relative phase, is calculated. Temperature effects are represented in Fig. 7 for the same parameters as in Fig. 2 and the interesting points of time $\tau = 7.1$ and $\tau = 9.0$ where the contrast maximally vanishes, reappears, respectively. As the experiments in Ref. [28] are performed in a temperature regime where only the three lowest-lying states are significantly populated, both statistical averages, over the three lowest-lying states and all states, are calculated. The curves for only the three lowest-lying and all states stay almost identical up to temperatures where $k_B T$ approximately equals the energy separation of the ground and the first excited states. The value of the QFI at $\tau = 7.1$ is still adequate, while the contrast stays low. Also, for $\tau = 9.0$, the signatures are not

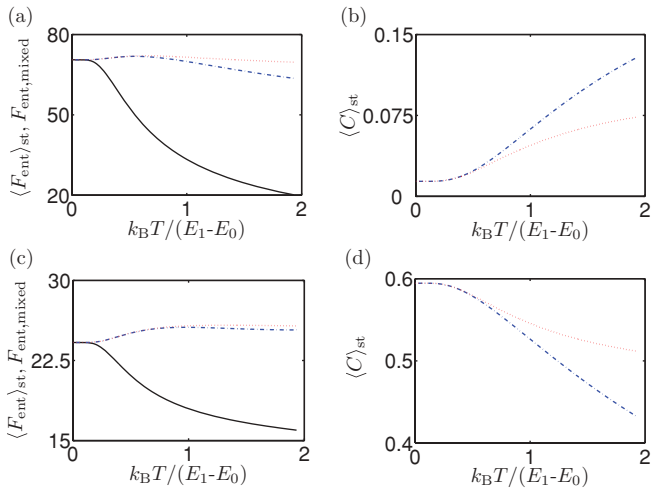

FIG. 7. (Color online) (a) $F_{\rm ent}$ for $\tau = 7.1$ and (c) $\tau = 9.0$. Black solid line: QFI $F_{\rm ent,mixed}$ for mixed states [cf. Eq. (18)], blue dashed line: $\langle F_{\rm ent}\rangle_{\rm st}$ statistically averaged over all 111 states, red dotted line: $\langle F_{\rm ent}\rangle_{\rm st}$ statistically averaged over the three lowest-lying experimentally important states [28]. (b) and (d): Contrast $\langle C\rangle_{\rm st}$ for $\tau = 7.1$ and $\tau = 9.0$ [cf. Eq. (16)]. Blue dashed-dotted line: statistical average over all states, red dotted line: statistical average over three lowest-lying eigenstates. Parameters same as in Fig. 3, $2\mu_1/\omega = 1.0$.

influenced very much. For higher temperatures, the QFI for mixed states deviates from the statistically averaged QFI of Eq. (17). Hence, it should be noted that the measurement of the variance of the particle number difference at higher temperatures is not equivalent to the measurement of the QFI for mixed states, while for low enough temperatures, both quantities lead to similar results.

VI. CONCLUSION

To summarize, the occurrence of entanglement on short time scales is observed for a BEC in a tilted double-well potential. For this system, on the mean-field level, the entanglement generation is accelerated in the vicinity of hyperbolic fixed points. The robustness of the entangled states under realistic experimental conditions is analyzed, and parameters are presented where the signatures QFI for the relative phase and contrast are found to be sufficiently stable. In conclusion, for the proposed parameters, the phase distribution of the entangled state measured in an experiment is expected to exhibit two clearly distinguishable maxima.

Our results are based upon the widely used two-mode approximation. An analysis of its limitations can be found, for example, in Ref. [53]. Nevertheless, the two-mode approximation has, especially for comparatively small interaction strengths, been found to describe many aspects of the experiments [28,33]. In addition to the investigation of extended models, the influence of particle losses is certainly an interesting aspect for future work.

ACKNOWLEDGMENTS

We thank M. Holthaus and M. Oberthaler for discussions. N.T. and B.G. acknowledge funding by the Studienstiftung des deutschen Volkes.

[1] H. Lignier, C. Sias, D. Ciampini, Y. Singh, A. Zenesini, O. Morsch, and E. Arimondo, Phys. Rev. Lett. **99**, 220403 (2007).
[2] C. Sias, H. Lignier, Y. P. Singh, A. Zenesini, D. Ciampini, O. Morsch, and E. Arimondo, Phys. Rev. Lett. **100**, 040404 (2008).
[3] E. Kierig, U. Schnorrberger, A. Schietinger, J. Tomkovic, and M. K. Oberthaler, Phys. Rev. Lett. **100**, 190405 (2008).
[4] A. Eckardt, T. Jinasundera, C. Weiss, and M. Holthaus, Phys. Rev. Lett. **95**, 200401 (2005).
[5] A. Eckardt, M. Holthaus, H. Lignier, A. Zenesini, D. Ciampini, O. Morsch, and E. Arimondo, Phys. Rev. A **79**, 013611 (2009).
[6] M. Grifoni and P. Hänggi, Phys. Rep. **304**, 229 (1998).
[7] C. E. Creffield and T. S. Monteiro, Phys. Rev. Lett. **96**, 210403 (2006).
[8] T. Jinasundera, C. Weiss, and M. Holthaus, Chem. Phys. **322**, 118 (2006).
[9] M. P. Strzys, E. M. Graefe, and H. J. Korsch, New J. Phys. **10**, 013024 (2008).
[10] W. Hai, C. Lee, and Q. Zhu, J. Phys. B **41**, 095301 (2008).
[11] C. F. Wildfeuer, A. P. Lund, and J. P. Dowling, Phys. Rev. A **76**, 052101 (2007).
[12] Y. Castin and J. Dalibard, Phys. Rev. A **55**, 4330 (1997).
[13] J. Ruostekoski, M. J. Collett, R. Graham, and D. F. Walls, Phys. Rev. A **57**, 511 (1998).
[14] J. I. Cirac, M. Lewenstein, K. Mølmer, and P. Zoller, Phys. Rev. A **57**, 1208 (1998).
[15] J. A. Dunningham and K. Burnett, J. Mod. Opt. **48**, 1837 (2001).
[16] A. Micheli, D. Jaksch, J. I. Cirac, and P. Zoller, Phys. Rev. A **67**, 013607 (2003).
[17] R. Bach and K. Rzazewski, Phys. Rev. Lett. **92**, 200401 (2004).
[18] K. W. Mahmud, H. Perry, and W. P. Reinhardt, J. Phys. B **36**, L265 (2003).
[19] C. Weiss and N. Teichmann, Laser Phys. Lett. **4**, 895 (2007).
[20] C. E. Creffield, Phys. Rev. Lett. **99**, 110501 (2007).
[21] D. R. Dounas-Frazer, A. M. Hermundstad, and L. D. Carr, Phys. Rev. Lett. **99**, 200402 (2007).
[22] G. Ferrini, A. Minguzzi, and F. W. J. Hekking, Phys. Rev. A **78**, 023606 (2008).
[23] C. Weiss and Y. Castin, Phys. Rev. Lett. **102**, 010403 (2009).
[24] A. I. Streltsov, O. E. Alon, and L. S. Cederbaum, Phys. Rev. A **80**, 043616 (2009).
[25] A. I. Streltsov, O. E. Alon, and L. S. Cederbaum, J. Phys. B **42**, 091004 (2009).
[26] D. Dagnino, N. Barberan, M. Lewenstein, and J. Dalibard, Nature Phys. **5**, 431 (2009).
[27] A. Sørensen, L. M. Duan, J. I. Cirac, and P. Zoller, Nature (London) **409**, 63 (2001).
[28] J. Esteve, C. Gross, A. Weller, S. Giovanazzi, and M. K. Oberthaler, Nature (London) **455**, 1216 (2008).

[29] Y. Li, Y. Castin, and A. Sinatra, Phys. Rev. Lett. **100**, 210401 (2008).
[30] V. Giovannetti, S. Lloyd, and L. Maccone, Science **306**, 1330 (2004).
[31] S. Haroche and J.-M. Raimond, *Exploring the Quantum—Atoms, Cavities and Photons* (Oxford University Press, Oxford, 2006).
[32] C. Weiss and N. Teichmann, Phys. Rev. Lett. **100**, 140408 (2008).
[33] M. Albiez, R. Gati, J. Folling, S. Hunsmann, M. Cristiani, and M. K. Oberthaler, Phys. Rev. Lett. **95**, 010402 (2005).
[34] A. Smerzi, S. Fantoni, S. Giovanazzi, and S. R. Shenoy, Phys. Rev. Lett. **79**, 4950 (1997).
[35] I. Lesanovsky, S. Hofferberth, J. Schmiedmayer, and P. Schmelcher, Phys. Rev. A **74**, 033619 (2006).
[36] F. Piazza, L. Pezzé, and A. Smerzi, Phys. Rev. A **78**, 051601(R) (2008).
[37] C. Lee, L.-B. Fu, and Y. S. Kivshar, Europhys. Lett. **81**, 60006 (2008).
[38] H. J. Lipkin, N. Meshkov, and A. J. Glick, Nucl. Phys. **62**, 188 (1965).
[39] G. J. Milburn, J. Corney, E. M. Wright, and D. F. Walls, Phys. Rev. A **55**, 4318 (1997).
[40] J. Guckenheimer and P. Holmes, *Nonlinear Oscillations, Dynamical Systems and Bifurcations of Vector Fields* (Springer, New York, 1983).
[41] S. Ghose, R. Stock, P. Jessen, R. Lal, and A. Silberfarb, Phys. Rev. A **78**, 042318 (2008).
[42] C. M. Trail, V. Madhok, and I. H. Deutsch, Phys. Rev. E **78**, 046211 (2008).
[43] C. Weiss and N. Teichmann, J. Phys. B **42**, 031001 (2009).
[44] L. Pezzé and A. Smerzi, Phys. Rev. Lett. **102**, 100401 (2009).
[45] Here, the observable $\vec{J}_{\vec{n}}$ from Ref. [44] is taken to be the particle number difference n_{12}. Hence, a QFI relative to the relative phase is calculated.
[46] Reference [17] suggests distinguishing the $N00N$ states of Eq. (1) from the corresponding statistical mixtures via center-of-mass measurements.
[47] M. Greiner, O. Mandel, T. Esslinger, T. Hänsch, and I. Bloch, Nature (London) **415**, 39 (2002).
[48] A. Sinatra and Y. Castin, Eur. Phys. J. D **8**, 319 (2000).
[49] S. Rong, W. Hai, Q. Xie, and Q. Zhu, Chaos **19**, 033129 (2009).
[50] A. E. Leanhardt, T. A. Pasquini, M. Saba, A. Schirotzek, Y. Shin, D. Kielpinski, D. E. Pritchard, and W. Ketterle, Science **301**, 1513 (2003).
[51] A. Sinatra and Y. Castin, Eur. Phys. J. D **4**, 247 (1998).
[52] L. Mandel and E. Wolf, *Optical Coherence and Quantum Optics* (Cambridge University Press, Cambridge, UK, 1995).
[53] K. Sakmann, A. I. Streltsov, O. E. Alon, and L. S. Cederbaum, Phys. Rev. Lett. **103**, 220601 (2009).